Nanoscale Res Lett (2010) 5:1480–1486
DOI 10.1007/s11671-010-9665-3

NANO EXPRESS

Investigation into Photoconductivity in Single CNF/TiO_2-Dye Core–Shell Nanowire Devices

Zhuangzhi Li · Caitlin Rochford · F. Javier Baca · Jianwei Liu · Jun Li · Judy Wu

Received: 26 April 2010 / Accepted: 3 June 2010 / Published online: 15 June 2010

Abstract A vertically aligned carbon nanofiber array coated with anatase TiO_2 (CNF/TiO_2) is an attractive possible replacement for the sintered TiO_2 nanoparticle network in the original dye-sensitized solar cell (DSSC) design due to the potential for improved charge transport and reduced charge recombination. Although the reported efficiency of 1.1% in these modified DSSC's is encouraging, the limiting factors must be identified before a higher efficiency can be obtained. This work employs a single nanowire approach to investigate the charge transport in individual CNF/TiO_2 core–shell nanowires with adsorbed N719 dye molecules in dark and under illumination. The results shed light on the role of charge traps and dye adsorption on the (photo) conductivity of nanocrystalline TiO_2 CNF's as related to dye-sensitized solar cell performance.

Keywords Photoconductivity · Nanowire · Titanium dioxide · Dye-sensitized solar cell · Core–shell

Z. Li
Department of Physics, Hebei Normal University and Hebei Advanced Thin Film Laboratory, 050016 Shijiazhuang, People's Republic of China

C. Rochford (✉) · J. Wu
Department of Physics and Astronomy, University of Kansas, Lawrence, KS 66045, USA
e-mail: caitlinr@ku.edu

F. Javier Baca
Los Alamos National Laboratory, Los Alamos, NM 87545, USA

J. Liu · J. Li
Department of Chemistry, Kansas State University, Manhattan, KS 66506, USA

Introduction

Recently, many efforts in solar cell development have employed nontraditional schemes that are different from the conventional planar semiconductor p-n junction design in order to focus on simplifying fabrication and decreasing cost while maintaining a competitive efficiency. Of these solar cell designs, the most promising is the dye-sensitized solar cell (DSSC), first reported in 1991 to have an efficiency of 7.1% [1]. Since then, the efficiency has been pushed to over 10% [2, 3], but the theoretical limit of 31% [4] for a single junction semiconductor photovoltaic device remains far from reach.

Many attempts have been made to improve the original DSSC design and circumvent its inherent limitations, especially the low conductivity of the disordered TiO_2 nanoparticle film and potential charge recombination at the TiO_2 surface [5, 6]. One promising approach is to replace the nanoparticle network with a vertically aligned nanotube [7–10] or nanowire [11–17] array, which provides the electrons with a direct, uninterrupted route to the anode. Even though this variation is expected to improve the performance, the efficiency of the modified DSSC typically remains in the <1–5% range. Many explanations have been proposed for why the above modifications have failed to improve the performance, including an insufficiently large surface area for dye adsorption compared to the nanoparticle film [8, 12], air trapped inside the nanotubes [9], and large series resistance between the nanostructure and the electrodes [7, 8]. A detailed analysis of the modified structures within the new designs is therefore desired and critical in order to elucidate the failure mechanisms and quantify their effects.

In order to achieve this, we propose a sequential method, which disassembles the modified DSSC in order to gather

information that cannot be obtained once a bulk device has been assembled. With this strategy, one can track the contribution of each component and identify which step or interface is most responsible for the poor performance. Further, each component can be optimized individually by making systematic and controlled modifications.

Core–shell nanowires of carbon nanofiber coated with anatase TiO_2 (CNF/TiO_2) will be the subject of this study. In a recent work, a vertically aligned CNF/TiO_2 nanowire array was employed to replace the sintered TiO_2 nanoparticle network [16]. The observation of complete fluorescence quenching suggests that the CNF readily accepts photoexcited electrons from the TiO_2 [17]. This allows the electrons to be transported through the higher-conductivity CNF core instead of the lower-conductivity TiO_2 shell, improving charge transport and decreasing recombination. Additionally, this structure offers an enhanced surface area for dye adsorption compared to traditional nanowires (NWs) due to the rough TiO_2 surface. Despite these expected improvements, the efficiency of the CNF/TiO_2 modified DSSC was much below that of the original DSSC. To understand the underlying physics behind the low efficiency, we have investigated charge transport properties and photoconductivity of single CNF/TiO_2-dye NW devices.

Experiment

The CNF/TiO_2 core–shell NW samples were prepared by depositing a particulate anatase TiO_2 film for 30 min at 500 °C onto a vertically aligned carbon nanofiber (VACNF) array by metal–organic chemical vapor deposition (MOCVD) [17]. The VACNFs used are a subset of multi-walled CNTs grown by plasma-enhanced chemical vapor deposition (PECVD) on silicon substrates [18–20]. The details of the growth have been described elsewhere [16, 17]. To fabricate individual CNF/TiO_2 core–shell NW devices as schematically shown in Fig. 1a, the as-grown NWs were dispersed into ethanol and transferred onto a silicon substrate covered with 500 nm thermally grown silicon dioxide. Bi-layer electron beam resist (PMMA/MMA-MAA) was used in the electron beam lithography (EBL) process for the definition of two or four electrodes. Before electrode deposition, a subset of the samples was treated with O_2 plasma at 20 W for 30 s via reactive ion

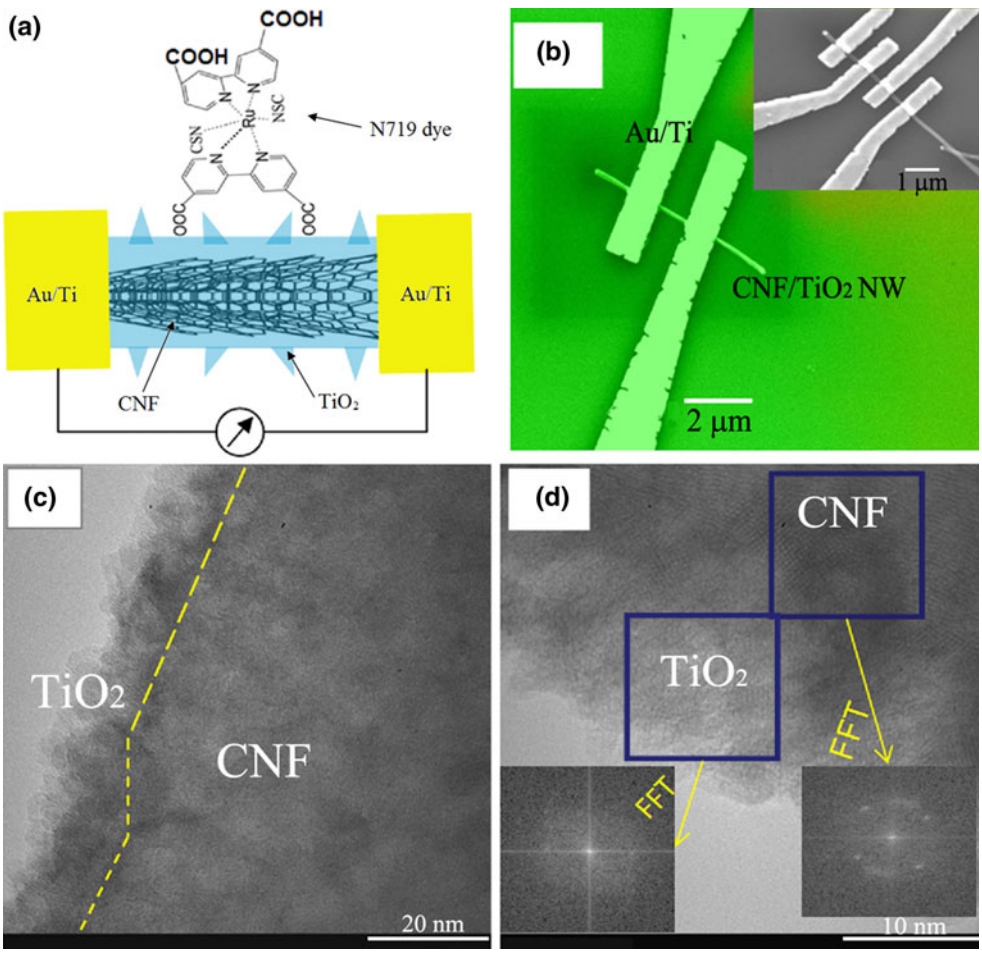

Fig. 1 **a** Schematic diagram of a single CNF/TiO_2 core–shell NW device. **b** SEM image of a device used in the study. *Inset* shows a four-probe device used to measure contact resistance and resistivity. **c** TEM image showing the core–shell structure of the CNF/TiO_2 NW. The *yellow dashed line* shows the interface between the TiO_2 shell and CNF core. **d** Microstructure of the core–shell NW, *insets* give the FFT results for the shell and core, respectively

etching (RIE) at a pressure of 7.1 mTorr in order to remove any possible residual electron beam resist and other surface contaminants that could prevent Ohmic contact between the electrodes and TiO_2 shell. Ti (15 nm)/Au (120 nm) electrodes were deposited by using electron beam evaporation through the EBL-defined mask followed by liftoff with acetone. After fabrication, all samples were annealed at 400 °C for 30 min with a temperature ramping rate of 15 °C/min. The annealing was performed in vacuum at a pressure of $\sim 10^{-5}$ Torr or better, with the intention of avoiding oxidation of Ti in the bottom layer of the electrode and desorbing any possible residual chemicals on the surface of the nanowire due to the above processes. To attach dye molecules onto the TiO_2 surface of the CNF/TiO_2 core–shell NW device, the O_2 plasma treated and untreated samples were soaked in 0.2 mM ethanol solution of cis-bis (isothiocyanoto) bis (2,2′-bipyridyl-4,4′-dicarboxylato)-ruthenium(II) bis- tetrabutylammonium dye (N719, Solaronix) for 12 h and blown dry with pure N_2. The soaking and mounting of the samples were performed in dark in order to limit the premature exposure of the devices to light. The prepared samples were enclosed in an aluminum box in order to measure the dark I–V characteristics before exposure to one sun illumination (100 mW/cm^2) produced by a solar simulator outfitted with an AM 1.5 G filter (Newport).

Results and Discussion

Figure 1a schematically depicts the structure of the CNF/TiO_2-dye core–shell NW device. It consists of a CNF/TiO_2 core/shell NW with two metal electrodes on the surface of the TiO_2 sheath. A scanning electron microscopy (SEM) image of a representative CNF/TiO_2 core/shell NW device is shown in Fig. 1b. The NW in the device has a stem length of ~ 4 μm. Additionally, a four-probe device is shown in the inset of Fig. 1b, which was fabricated to measure the contact resistance between the metal probes and the NW. The CNF core of the NW has an average diameter of ~ 100 nm, while the TiO_2 sheath of the samples used in this study is about 10–15 nm thick [17]. The microstructures and morphologies of the CNF/TiO_2 core–shell NW were studied using high-resolution transmission electron microscopy (HRTEM). As shown in Fig. 1c, TiO_2 forms a conformal particulate film surrounding the CNF core, covering the CNF core uniformly even at a kink of the CNF, which is shown by the dashed line at the interface of the core and shell. Fast Fourier Transform (FFT) was used to analyze the crystalline structure of CNF core and TiO_2 shell. Distinct ordered planes as suggested by the discrete spots were observed on CNF (right inset of Fig. 1d), while a mixture of compact fine grains several nanometers in size embedded in an amorphous phase was suggested for the TiO_2 sheath (left inset of Fig. 1d). X-ray diffraction analysis on CNF/TiO_2 NW array indicates the fine grains are anatase TiO_2 [17]. HRTEM suggests the dimension of the grains is in the range of 3-5 nm.

Figure 2a shows the *I–V* characteristics of Sample *d1*, which is a representative in a group of six samples not treated with O_2 plasma, in dark and under illumination before and after dye attachment. Although only the positive bias is shown, it should be noted that the curve is symmetric. Contact resistance in the range of 3–8 MΩ was typically observed for the untreated samples. As previously mentioned, this large contact resistance is likely due to a contaminated TiO_2 surface, which may prevent Ohmic contact between Ti and TiO_2 during metal evaporation and the diffusion of Ti to TiO_2 during annealing. Before dye attachment, Sample *d1* exhibits a considerably high dark current (open black circles). This may be attributed to the large number of dangling bonds and the interfaces in the amorphous TiO_2 phase and between crystallites and amorphous TiO_2 phase in the TiO_2 sheath. The resulting high density of oxygen vacancies may act as electron donors and therefore cause substantial dark current. The illuminated current (open red circles) is only slightly higher than the dark current before dye attachment, which may contain direct band transition in the TiO_2 ($E_g \sim 3.4$ eV) close to the UV end of the solar spectrum and sub-band

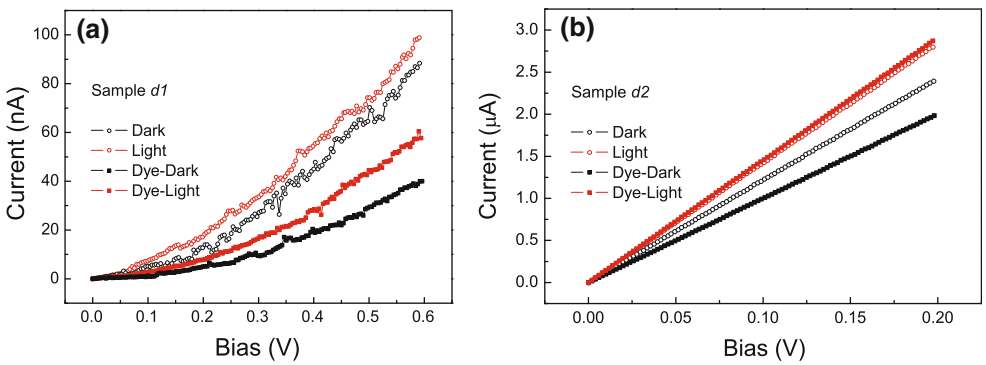

Fig. 2 **a** Dark and illuminated I–V curves for Sample *d1* without and with dye and **b** the corresponding curves for Sample *d2*

transition of TiO_2. The sub-band transition is commonly seen in nanostructured TiO_2 and is due to localized defect-induced band gap states. Furthermore, the measurement on uncoated individual CNF samples (not shown) exhibits no photoresponse under the conditions presented in this paper, suggesting the observed photoresponse is due to the TiO_2 or dye only.

After attaching dye molecules, the dark (solid black squares) and illuminated (solid red squares) current of Sample *d1* decreased noticeably as shown in Fig. 2a. We speculate that the decrease is due to the passivation of some hole traps during the dye attachment. The current decrease may then be explained in the following way. It has been suggested that non-equilibrium holes rapidly become trapped in deep traps, which may be concentrated in particular regions due to inhomogeneity in the lattice such as grain boundaries. These traps produce a local potential barrier that prohibits electrons from readily recombining with the holes, thus separating charge carriers and improving conductivity [21]. The N719 dye is expected to attach to the TiO_2 surface via its carboxyl group [22]. While the sample is soaking in solution, the protons that previously resided on the now negatively charged carboxyl group may passivate some of the hole traps near the surface. These hole traps are commonly associated with oxygen vacancies, which can readily occur on the surface as well as at the grain boundaries within the nanocrystalline/amorphous TiO_2.

Even though both the dark and illuminated currents decreased, the photo-induced current, defined as the difference between the illuminated and dark currents at a particular bias, increased after dye attachment. This suggests that the dye molecules do in fact contribute to the photo-induced current, or more specifically, the free electron density. This may occur in three ways. First, the dye molecules may inject photo-excited electrons into the TiO_2 layer and increase the electron density. It should be recognized that dye regeneration may not occur effectively in this case due to absence of the electrolyte, so this mechanism is not expected to contribute to the measured current. Second, the presence of the dye molecules may modify the number of the hole traps, as argued earlier. This mechanism will be demonstrated further via transient photoconductivity measurements. Third, since the measurements occur in air, which contains molecular oxygen, a known electron scavenger [23], the presence of the dye molecules may block some of the molecular oxygen from removing conduction electrons and forming adsorbed O_2^- sites that decreases the free electron density in the TiO_2. Measurements of single CNF/TiO_2 nanowires in vacuum (not shown) exhibit a current that is 1–2 orders of magnitude higher than in air. This is in qualitative agreement with studies on thin films of nanocrystalline TiO_2 [24, 25] in which environments containing lower oxygen content resulted in higher current due to the decreased number of electron scavengers. This suggests that blocking access to the surface of the TiO_2 would have a similar effect and thus increase the electron concentration and hence current.

The I–V measurements were repeated on Sample *d2*, which is representative of the samples with electrode contact area treated with O_2 plasma before electrode deposition. The O_2 plasma treatment improved the electrical contact to the CNF/TiO_2 NW considerably as shown in Fig. 2b. From four-probe measurements, the contact resistance of the treated samples is several to several tens of kΩ, which is two to three orders of magnitude smaller than that of the untreated samples. The resistivity of Sample *d2* is estimated to be $(6.4 \pm 2.1) \times 10^{-2}$ Ω cm. This value seems reasonable since it lies between the intrinsic resistivity of CNF ($0.4–7 \times 10^{-3}$ Ω cm [26–28]) and that of TiO_2 thin films (2.6×10^{-1}–10^6 Ω cm [29, 30]). The low resistivity of the core–shell nanowire compared to thin film TiO_2 suggests that the CNF does in fact contribute to the charge transport even when both electrical contacts are on the TiO_2 shell. This indicates low resistance across the CNF/TiO_2 interface. This low-resistance interface may be understood from the growth chemistry of the TiO_2 shell on CNF. During PECVD, a mixture of C_2H_2 (at 62 sccm) and NH_3 (at 252 sccm) was used as gas precursor. Particularly, the NH_3 content is about four times that of C_2H_2. This generates an important plasma etching effect to remove the amorphous carbon, which may be deposited at the CNF surface. For many carbon nanotube studies, the amorphous carbon has been the major factor affecting the interface properties. The hydrogen atoms covalently bonded to the CNF surface at the graphitic edge do not seem to be a problem. Four-probe electrical measurements with side contact by Zhang et al. [28] did not show any evidence of an interface problem. In addition, during MOCVD of TiO_2, the oxygen atoms involved in the reaction will likely react with hydrogen and form a C–O bond before TiO2 is deposited. The I–V characteristics become more linear after O_2 plasma treatment, which indicates an Ohmic contact on the metal–semiconductor interface. The reduction of the contact resistance results in a significant current enhancement of almost two orders of magnitude both in dark and under illumination when compared to the untreated Sample *d1*. In addition, the photo-induced current in Sample *d2* is significantly higher than in *d1*. At 100 mV bias, the photo-induced current in Sample *d2* is ~0.21 μA after dye attachment, which is about two orders of magnitude higher than in the untreated samples. This result confirms that an Ohmic contact to the nanostructured materials is essential to the charge transport in a NW device [31, 32].

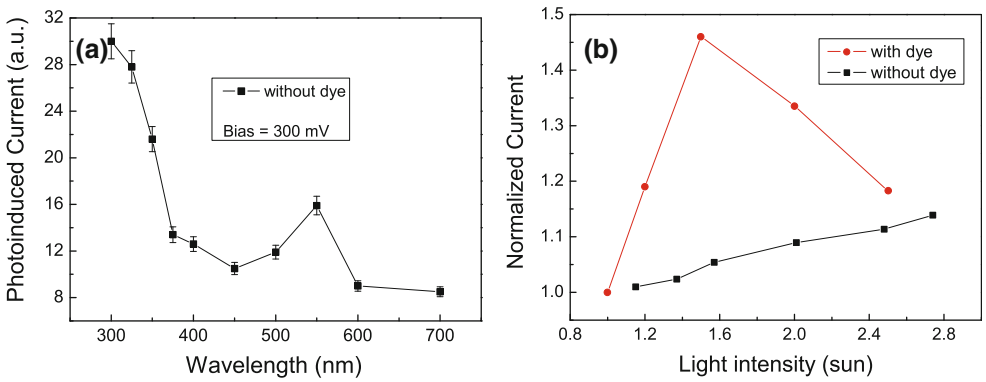

Fig. 3 Photo-induced current at constant bias for a single CNF/TiO_2 NW device as a function of **a** incident light wavelength and **b** light intensity

The O_2 plasma treatment was also applied to the TiO_2–dye interface in order to examine if a similar residue or interface layer was present that could hinder dye adsorption. To make a direct comparison, the dye was removed from Sample *d2* before it was subjected to O_2 plasma cleaning under the same processing conditions mentioned earlier except for a longer processing time of 1 min. Immediately after the treatment, the sample showed an enhanced photo-induced current that decayed back after 12 h in the dark in air. Dye was then attached using the previously described method, and the photo-induced current recovered more or less the original value shown in Fig. 2. This observation suggests that the surface of the TiO_2 was clean with respect to dye attachment. It remains a question whether such plasma cleaning benefits electron transfer from dye to TiO_2 in the presence of electrolyte.

The spectral dependence of the photo-induced current (Sample *d2*) before dye attachment is illustrated in Fig. 3a. Two peaks are clearly visible. The first is at wavelengths smaller than 375 nm, which corresponds to a bandgap of ~3.3 eV and is within the reported range for nanocrystalline TiO_2 [33]. The second peak appears around 550 nm, which has been observed on TiO_2 nanoparticles and is attributed to the sub-band transitions [17]. Interestingly, no such peak was observed on the photoluminescence curve measured on TiO_2/CNF array with 60 min of TiO_2 growth time [17], as opposed to 30 min for the samples used in this work. A plausible explanation is the much improved crystallinity in TiO_2 layer with longer growth time, which resulted in much reduced sub-band charge carriers. On the other hand, the direct transport measurement employed in this work may provide higher sensitivity than the optical one. As we mentioned earlier, the possible contribution of the CNF core to the spectral feature of the photo-induced current can be ruled out. In fact, the same spectral current measurement was repeated on individual CNF devices, and no photo-induced current was observed.

Figure 3b shows the photo-induced current (normalized to that at 1 Sun) for Sample *d2* with and without dye as a function of incident light intensity. Before dye attachment, the current increases linearly with the light intensity, which indicates the carriers excited in TiO_2 is proportional to the number of incident photons. However, after dye molecules were attached to the NW, the photo-induced current versus light intensity curve experienced a dramatic drop at a light intensity of around 1.5 suns. This phenomenon may be attributed to the bleaching effect of dye molecules. After dye molecules were damaged above a certain light intensity, they may be detached from the TiO_2 surface. Based on the above discussion, this would reintroduce many electron traps and open up the TiO_2 surface to electron scavenging by molecular oxygen leading to a decrease in the number of free electrons.

While the previously mentioned I–V measurements were made under steady state conditions, the samples in fact exhibit a transient response to either the introduction or removal of incident light. The presence of transient photoconductivity is well documented in nanocrystalline TiO_2 thin films [24, 25, 33], but is interesting to observe in a single NW. In this measurement, the samples were first exposed to one sun illumination at a constant bias of 100 mV. The high surface-to-volume ratio and thus high density of electron traps due to hydroxylated surface Ti sites [34] prevents achievement of steady state current until all traps are filled and equilibrium is reached between trapping and de-trapping events. It was observed (not shown) that after dye attachment, the time required to reach steady state current was reduced by approximately 75%. This suggests that the dye molecules may passivate many of the hydroxylated surface Ti sites and greatly reduce the number of electron traps. However, since nearly 1 min is still required to reach steady state current after dye molecules are attached, it is likely that many potential dye adsorption sites remain and the dye loading is not optimized. Once a steady state current was achieved, the incident light was removed and the photo-induced current decay was recorded. Figure 4 shows the normalized photo-induced current decay profile in log–log and linear scale (inset) for samples without and with attached dye molecules. The mechanism responsible for the observed slow

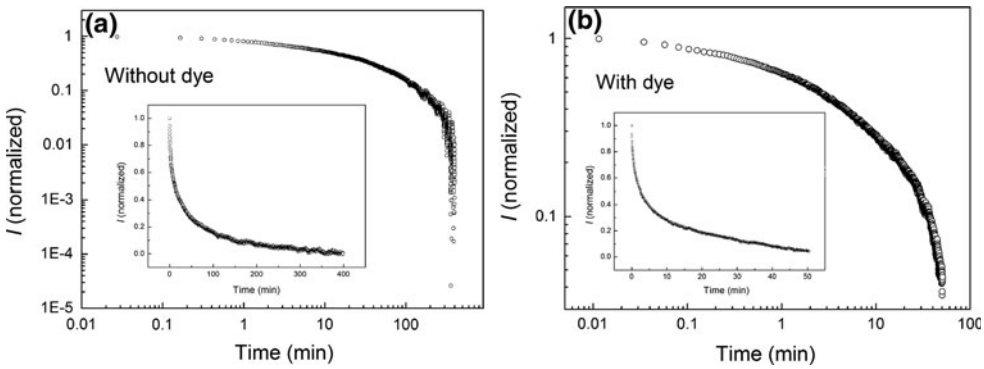

Fig. 4 Normalized photo-induced current decay of Sample *d*2 **a** without dye and **b** with dye. *Inset* shows the same data on a linear scale

current decay may be described as follows. As previously mentioned, under illumination, nonequilibrium holes become trapped in deep traps due to oxygen vacancies leading to an excess electron density equal to the trapped hole density [35]. These traps are assumed to be concentrated in certain regions due to inhomogeneities such as grain boundaries. This leads to local electric fields that spatially separate charge carriers and require electrons to overcome a potential barrier in order to recombine [21]. As time goes on, the separation between the quasi Fermi levels increases causing the recombination time to increase along with it. As can be seen in Fig. 4, the decrease in current is immediate and initially very fast followed by a much slower leveling off as the probability for the electron capture by tunneling through surface and inter-grain potential barriers decreases, which is consistent with previous work done on nanocrystalline TiO_2 thin films [25]. It can be clearly seen that the photoconductivity decay is more rapid when the dye is present. This is consistent with the above observations that the dye attachment passivates some hole traps on the surface. As the number of hole traps decreases, the recombination time also decreases [25].

Conclusion

In conclusion, electrical conductivity has been investigated on individual CNF/TiO_2 core–shell NW attached with N719 dye molecules in dark and under illumination. It has been found that the contact resistance to the TiO_2 surface may sensitively affect the dark and photo-induced conductivity by nearly two orders of magnitude, suggesting that care must be taken to ensure Ohmic contact between the TiO_2 structure and the anode in the DSSC. The nanocrystalline state of the TiO_2 shell affects both spectral and dynamic behaviors of the conductivity due to the presence of the defect-induced bandgap states and hole traps such as oxygen vacancies. The dye attachment reduces such an effect by passivating some of the vacancies at low illumination intensity up to 1.5 suns, above which damage to and subsequent detachment of the dye molecule may occur. The single nanowire approach presented in this work may be applied to many nanostructures involved in nanostructured DSSC and other optoelectronic devices to achieve an understanding of the electrical transport at the nanoscale.

Acknowledgments The authors acknowledge support from the NSF EPSCoR for this work. CR recognizes a NSF Graduate Research Fellowship. JW is supported in part by ARO and NSF. JL also thanks Kansas State University for financial support.

References

1. B. O'Regan, M. Gratzel, Nature **353**, 737 (1991)
2. A. Hagfeldt, M. Gratzel, Acc. Chem. Res. **33**, 269 (2000)
3. M. Grätzel, J. Photochem. Photobiol. A **164**, 3 (2004)
4. W. Shockley, H.J. Queisser, J. Appl. Phys. **32**, 510 (1961)
5. M. Gratzel, Nature **414**, 338 (2001)
6. M. Grätzel, J. Photochem. Photobiol. C **4**, 145 (2003)
7. K. Zhu, N.P. Neale, A. Miedaner, A.J. Frank, Nano Lett. **7**, 69 (2007)
8. G.K. Mor, K. Shankar, M. Paulose, O.K. Varghese, C.A. Grimes, Nano Lett. **6**, 215 (2006)
9. M. Paulose, K. Shankar, O.K. Varghese, G.K. Mor, B. Hardin, C.A. Grimes, Nanotechnology **17**, 1446 (2006)
10. C. Lin, W. Yu, S. Chien, Appl. Phys. Lett. **93**, 133107 (2008)
11. M. Law, L.E. Greene, J.C. Johnson, R. Saykally, P. Yang, Nat. Mater. **4**, 455 (2005)
12. J.B. Baxter, E.S. Aydil, Appl. Phys. Lett. **86**, 053114 (2005)
13. K. Lee, C. Hu, H. Chen, K. Ho, Sol. Energy Mater. Sol. Cells **92**, 1628 (2008)
14. A. Kongkanand, R.M. Dominguez, P.V. Kamat, Nano Lett. **7**, 676 (2007)
15. Z. Yang, T. Xu, Y. Ito, U. Welp, W.K. Kwok, J. Phys. Chem. C **113**, 20521 (2009)
16. J. Liu, Y.T. Kuo, K.J. Klabunde, C. Rochford, J. Wu, J. Li, ACS Appl. Mater. Interfaces **1**, 1645 (2009)
17. J. Liu, J. Li, A. Sedhain, J. Lin, H. Jiang, J. Phys. Chem. C **112**, 17127 (2008)
18. B.A. Cruden, A.M. Cassell, Q. Ye, M. Meyyappan, J. Appl. Phys. **94**, 4070 (2003)

19. M.S. Haque, K.B.K. Teo, N.L. Rupensinghe, S.Z. Ali, I. Haneef, S. Maeng, J. Park, F. Udrea, W.I. Milne, Nanotechnology **19**, 025607 (2008)
20. Z.F. Ren, Z.P. Huang, J.W. Xu, J.H. Wang, P. Bush, M.P. Siegal, P.N. Provencio, Science **282**, 1105 (1998)
21. M. Sheinkman, A.Y. Shik, Sov. Phys. Semicond. **10**, 128 (1976)
22. H. Fumihiko, K. Koei, S. Takahiko, N. Yuzuru, K. Yasuo, N. Michio, Electrochem. Solid-State Lett. **11**, A109 (2008)
23. W. Göpel, G. Rocker, R. Feierabend, Phys. Rev. B **28**, 3427 (1983)
24. J. Nelson, A. Eppler, I. Ballard, J. Photochem. Photobiol. A **148**, 25 (2002)
25. K. Pomoni, A. Vomvas, C. Trapalis, Thin Solid Films **479**, 160 (2005)
26. J. Li, Q. Ye, C. Alan, H.T. Ng, S. Ramsey, J. Han, M. Meyyappan, Appl. Phys. Lett. **82**, 2491 (2003)
27. Q. Ngo, A.M. Cassell, A.J. Austin, J. Li, S. Krishnan, M. Meyyappan, C.Y. Yang, IEEE Electron Device Lett. **27**, 221 (2006)
28. L. Zhang, D. Austin, V.I. Merkulov, A.V. Meleshko, K.L. Klein, M.A. Guillorn, D.H. Lowndes, M.L. Simpson, Appl. Phys. Lett. **84**, 3972 (2004)
29. T. Miyata, S. Tsukada, T. Minami, Thin Solid Films **496**, 136 (2006)
30. R. Könenkamp, A. Wahi, P. Hoyer, Thin Solid Films **246**, 13 (1994)
31. J. Zhou, Y. Gu, Y. Hu et al., Appl. Phys. Lett. **94**, 191103 (2009)
32. J. Appenzeller, M. Radosavljevic, J. Knoch, Ph. Avouris, Phys. Rev. Lett. **92**, 048301 (2004)
33. D. Comedi, S.P. Heluani, M. Villafuerte, R.D. Arce, R.R. Koropecki, J. Phys. Condens. Matter **19**, 486205 (2007)
34. S.H. Szczepankiewicz, A.J. Colussi, M.R. Hoffmann, J. Phys. Chem. B **104**, 9842 (2000)
35. S.A. Studenikin, N. Golego, M. Cocivera, J. Appl. Phys. **87**, 2413 (2000)